*Journal of The Electrochemical Society*, **158** (3) A250-A254 (2011)
0013-4651/2011/158(3)/A250/5/$28.00 © The Electrochemical Society

# Mg and Fe Co-doped Mn Based Olivine Cathode Material for High Power Capability

**Jongsoon Kim,[a] Young-Uk Park,[a] Dong-Hwa Seo,[a] Jinsoo Kim,[b] Sung-Wook Kim,[d] and Kisuk Kang[a,b,c,*,z]**

[a]*Department of Materials Science and Engineering,* [b]*Graduate School of Energy, Environment, Water and Sustainability, and* [c]*Korea Advanced Institute of Science and Technology Institute for Eco-Energy and Nanocentury, Korea Advanced Institute of Science and Technology, Yuseong-gu, Daejeon 305-701, Korea*
[d]*Research Institute of Advanced Materials, Seoul National University, Gwanak-gu, Seoul 151-742, Korea*

Here we demonstrate that the electrochemical properties of Mn based olivine cathode materials can be significantly improved by small amount of co-dopants, Fe and Mg. While nucleation and growth are important in determining the kinetics of a two-phase reaction based olivine electrode, the presence of Fe and Mg in $LiMnPO_4$ framework notably enhances the power capability of a $LiMnPO_4$ electrode providing multiple nucleation sites. The electrochemical activity of an Fe–Mg co-doped Mn olivine cathode material measured by galvanostatic charge/discharge indicates that a discharge capacity of about 140 mAh $g^{-1}$ can be obtained at a C/5 rate and this high capacity is retained at even higher current rates (110 mAh $g^{-1}$ at 3C), which has yet to be achieved in $LiMnPO_4$ without nucleation enhancers.
 [DOI: 10.1149/1.3524260] 

Manuscript received November 1, 2010. Published January 5, 2011.

Olivine $LiMPO_4$ (M = Fe, Mn, Co, Ni) have been highlighted as potential cathode materials owing to their relatively high structural stability and high theoretical capacity ( ~ 170 mAh $g^{-1}$).[1-3] Among olivine structure materials, $LiFePO_4$ has been extensively studied as the potential cathode on the basis of its numerous appealing features such as potentially low cost and safety.[4-9] However, due to the intrinsic problem of low energy density resulting from a low $Fe^{2+}/Fe^{3+}$ redox potential of ca. 3.4 V, new attention has been directed to $LiMnPO_4$, which offers an operating potential of $Mn^{2+}/Mn^{3+}$ redox potential of ca. 4.1 V.[2,10-14] Because the operating voltage of $LiMnPO_4$ is similar to that of $LiCoO_2$, presently the most widely used cathode, it is anticipated that replacement of the cathode with this material can be accomplished without major difficulties at the battery system level. Also, the availability of Mn in nature corresponds with that of Fe. Therefore, intensive research efforts have been focused on this material.[13-30] However, despite these promising aspects, the inferior kinetic property of $LiMnPO_4$ remains a major obstacle toward its application. As a result, the theoretical electrochemical properties of $LiMnPO_4$ have yet to be achieved, even under mild operation conditions.

Recently, our group demonstrated that the power capability of $LiFe_{0.05}Co_{0.05}Mn_{0.9}PO_4$ can be significantly improved over pristine $LiMnPO_4$ due to the role of Co and Fe in the structure.[15] In the present work, we further show that small amounts of co-doping of Fe–Mg can also serve as a nucleation enhancer in $LiMnPO_4$ framework. Unfavorable $Fe^{3+}$–$Mn^{2+}$ pairs during charging and unfavorable $Mg^{2+}$–$Mn^{3+}$ pairs during discharging can make $Mn^{2+}/Mn^{3+}$ transition more facile promoting the nucleation of the second phase. Compared to pristine $LiMnPO_4$, the electrochemical properties of $LiFe_{0.05}Mg_{0.05}Mn_{0.9}PO_4$ are shown to be remarkably improved by nucleation enhancers during (de)lithiation.

## Experimental

$LiMnPO_4$ and $LiFe_{0.05}Mg_{0.05}Mn_{0.9}PO_4$ samples were prepared through a sol–gel synthesis. A stoichiometric amount of $Li(CH_3COO)\cdot 2H_2O$, $Mn(CH_3COO)_2$, $Fe(CH_3COO)_2$, $Mg(CH_3COO)_2\cdot 4H_2O$, and $NH_4H_2PO_4$ precursors was dissolved in deionized water with glycolic acid and $HNO_3$ to form the sol state. This solution was heated to 70°C for 12 h. The precursors were then fired at 350°C under an Ar condition for 3 h, reground, and manually pelletized. After preheating, we calcined the pellet at 520°C under an Ar condition for 3 h.

For the electrochemical characterization, the active materials were dry ballmilled with 20 wt % carbon black (Super-P) for 24 h. A slurry of 80 wt % carbon-coated $LiMnPO_4$ and $LiFe_{0.05}Mg_{0.05}Mn_{0.9}PO_4$, 11 wt % carbon black (Super-P), and 9 wt % polyvinylidene fluoride dispersed in N-methy1-2-pyrrolidone (NMP) was prepared and cast on aluminum foil. NMP was evaporated at 70°C for 12 h. Electrochemical cells were assembled in a CR2016 type coin cell with a Li counter electrode, separator (Celgard 2400), and 1 M $LiPF_6$ electrolyte in a mixture of 1:1 ethyl carbonate/dimethyl carbonate in an Ar-filled glove box. The charge/discharge test was performed using a potentiostat-galvanostat (WonA Tech). Partially delithiated samples were prepared by carefully retrieving the electrode from coin cells at different charge states. The electrodes were washed with dimethyl carbonate and dried in a vacuum before being used in X-ray diffraction (XRD, Rigaku D/Max 2500) analyses. In the potentiostatic intermittent titration technique (PITT) measurements, a "staircase" voltage profile was used in which the cell voltage was raised in 5 mV increments. The current versus time, $I(t)$, was measured at constant potential at 0.05–0.2 s intervals depending on the rate of current decay. Each individual titration was terminated when the absolute current reached a C/50 rate.

## Results and Discussion

A schematic picture of proposed (de)lithiation mechanism in the olivine system doped with nucleation enhancers is illustrated in Fig. 1.[15] When small amounts of Fe and Mg are substituted in Mn sites, the initial delithiation occurs by the oxidation of $Fe^{2+}$ to $Fe^{3+}$ because of the lower $Fe^{2+}/Fe^{3+}$ redox potential ( ~ 3.4 V) relative to the $Mn^{2+}/Mn^{3+}$ redox potential ( ~ 4.1 V) during charging. At this state, vacancies are likely to be more populated around Fe due to the attractive interaction of $Fe^{3+}$–$V_{Li}$ (effectively $h^+$–$e^-$).[15,31,32] Because Fe is dilute in this system, the generation of $Fe^{3+}$–$V_{Li}$ will result in $Mn^{2+}$–$V_{Li}$ (effectively $e^-$–$e^-$) in neighbors. With further delithiation after full oxidation of $Fe^{2+}$ to $Fe^{3+}$, $Mn^{2+}$ in the $Mn^{2+}$–$V_{Li}$ neighbor will most likely be oxidized to $Mn^{3+}$ because there is energetic gain in the transition from $Mn^{2+}$–$V_{Li}$ ($e^-$–$e^-$) repulsion to $Mn^{3+}$–$V_{Li}$ ($h^+$–$e^-$) attraction. In contrast, the oxidation of $Mn^{2+}$, when solely surrounded by $Mn^{2+}$–$Li^+$ pairs, will not have energetic gain in the transition from $Mn^{2+}$–$Li^+$ (effectively $e^-$–$h^+$) attraction to $Mn^{3+}$–$V_{Li}$ ($h^+$–$e^-$) attraction. Therefore, the $Mn^{2+}/Mn^{3+}$ transition will be initiated mostly from Fe-containing regions, where subsequently $V_{Li}$ is

* Electrochemical Society Active Member.
z E-mail: matlgen1@kaist.ac.kr

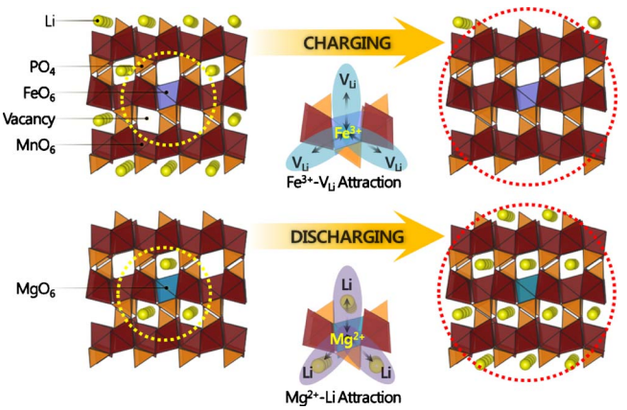


**Figure 1.** (Color online) Schematic illustration of the nucleation enhancing process in a multicomponent Mn based olivine cathode during charging and discharging (Yellow: Li, red: $MnO_6$, purple: $FeO_6$, blue: $MgO_6$, orange: $PO_4$, white: vacancy). Arrows are used to indicate the favorable interaction.

further populated due to the attraction between $M^{3+}$ and $V_{Li}$. This region will serve as nuclei of the delithiated phase in the charge process [Fig. 1 (top)]. Because Fe is extensively spread in the framework, multiple nucleation sites of the delithiated phase can form within a single particle.

A similar effect can be expected during lithiation by substituting Mg into Mn sites. In a highly charged state with full oxidation of $Fe^{3+}$ and $Mn^{3+}$, remaining $Li^+$ in the structure will be mostly populated around $Mg^{2+}$ due to the effective repulsion between $Li^+$ and $Fe^{3+}$ or $Mn^{3+}$. Because Mg is dilute in the Mn-rich structure, the presence of $Li^+$–$Mg^{2+}$ pairs will also introduce unfavorable $Mn^{3+}$–$Li^+$ ($h^+$–$h^+$) pairs in the vicinity. With discharge, these unfavorable $Mn^{3+}$–$Li^+$ pairs can readily promote the $Mn^{3+}/Mn^{2+}$ transition near $Mg^{2+}$ becoming $Mn^{2+}$–$Li^+$ ($e^-$–$h^+$) pairs [Fig. 1 (bottom)]. This region with $Mg^{2+}$ will initiate nucleation of the lithiated phase in the discharge process.

Motivated by this nucleation enhancer concept in Mn based olivine both at the charge and discharge processes, we have prepared Fe and Mg co-doped $LiFe_{0.05}Mg_{0.05}Mn_{0.9}PO_4$ and compared its property with the pristine $LiMnPO_4$.[15] Figure 2 shows XRD patterns of the $LiMnPO_4$ and $LiFe_{0.05}Mg_{0.05}Mn_{0.9}PO_4$. All materials show standard diffraction patterns of the olivine *Pmnb* space group without any contamination or second phases. The Rietveld refinement tabulated in Table I reveals that the three lattice parameters of pure $LiMnPO_4$ are $a$ = 6.115 Å, $b$ = 10.463 Å, and $c$ = 4.755 Å, which agree well with previous reports.[29] Those of $LiFe_{0.05}Mg_{0.05}Mn_{0.9}PO_4$ are $a$ = 6.087 Å, $b$ = 10.420 Å, and $c$ = 4.736 Å. A slight difference in the lattice parameters between $LiMnPO_4$ and $LiFe_{0.05}Mg_{0.05}Mn_{0.9}PO_4$ was observed. This is believed to be due to the differences of the ionic radii of $Mn^{2+}$, $Fe^{2+}$, and $Mg^{2+}$ ($Mn^{2+} > Fe^{2+} > Mg^{2+}$) and indicates that Fe and Mg are well incorporated in the olivine crystal.[25] $Mg^{2+}$ is found to be substituted mostly to the transition metal site (M2 site), not to the Li site (M1 site) from the Rietveld refinement, as shown in Table II. The particle sizes and morphologies of the two samples are similar as shown in Fig. 3, implying that the possible difference in electrochemical performance does not originate from external factors such as particle size. Also the carbon content analysis showed negligible difference between samples.

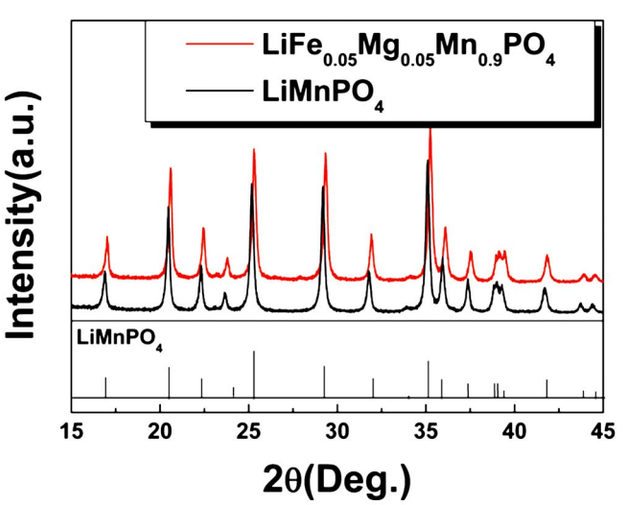


**Figure 2.** (Color online) XRD patterns and lattice parameter of $LiMnPO_4$ and $LiFe_{0.05}Mg_{0.05}Mn_{0.9}PO_4$ between 2θ = 15° and 2θ = 45°.

**Table I. Lattice parameters of $LiMnPO_4$ and $LiFe_{0.05}Mg_{0.05}Mn_{0.9}PO_4$ obtained by the Rietveld refinement.**

| | $a$ (Å) | $b$ (Å) | $c$ (Å) |
|---|---|---|---|
| $LiMnPO_4$ | **6.115** | **10.463** | **4.755** |
| $Li(FeMg)_{0.05}Mn_{0.9}PO_4$ | **6.087** | **10.420** | **4.736** |

The electrochemical performances of the two samples in Li cells are compared in Fig. 4. First, the rate capability of each sample is compared by charging the cells to 4.8 V constant current and constant voltage (CCCV) mode, C/20 and 2 h holding and discharging at various rates. The cells were discharged at rates from C/5 to 3C as shown in Fig. 4a. It is clear that $LiFe_{0.05}Mg_{0.05}Mn_{0.9}PO_4$ can deliver significantly higher capacities than $LiMnPO_4$ at all current rates. At C/5, the specific capacity of $LiFe_{0.05}Mg_{0.05}Mn_{0.9}PO_4$ is approximately 140 mAh $g^{-1}$, whereas $LiMnPO_4$ can only deliver ca. 100 mAh $g^{-1}$. The ca. 4.1 V plateau is more clearly observed for $LiFe_{0.05}Mg_{0.05}Mn_{0.9}PO_4$, indicating enhanced kinetic behavior at this current rate. Furthermore, the discharge capacities of

**Table II. Site occupancies of $LiFe_{0.05}Mg_{0.05}Mn_{0.9}PO_4$ obtained by the Rietveld refinement.**

| Name | Type | Occupancy (theoretical) | Occupancy (experimental) |
|---|---|---|---|
| Li1 | $Li^{+1}$ | 1 | 0.9988 |
| Li2 | $Li^{+1}$ | 0 | 0.0012 |
| Mg1 | $Mg^{+2}$ | 0 | 0.0012 |
| Mg2 | $Mg^{+2}$ | 0.05 | 0.0488 |
| Fe1 | $Fe^{+2}$ | 0.05 | 0.05 |
| Mn1 | $Mn^{+2}$ | 0.9 | 0.9 |
| P | $P^{+5}$ | 1 | 1 |
| O1 | $O^{-2}$ | 1 | 1 |
| O2 | $O^{-2}$ | 1 | 1 |
| O3 | $O^{-2}$ | 1 | 1 |
| O4 | $O^{-2}$ | 1 | 1 |

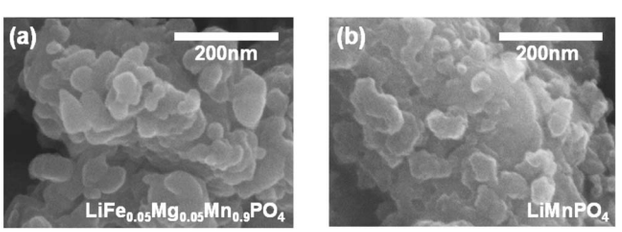


**Figure 3.** Scanning electron microscopy images of (a) $LiMnPO_4$ and (b) $LiFe_{0.05}Mg_{0.05}Mn_{0.9}PO_4$.

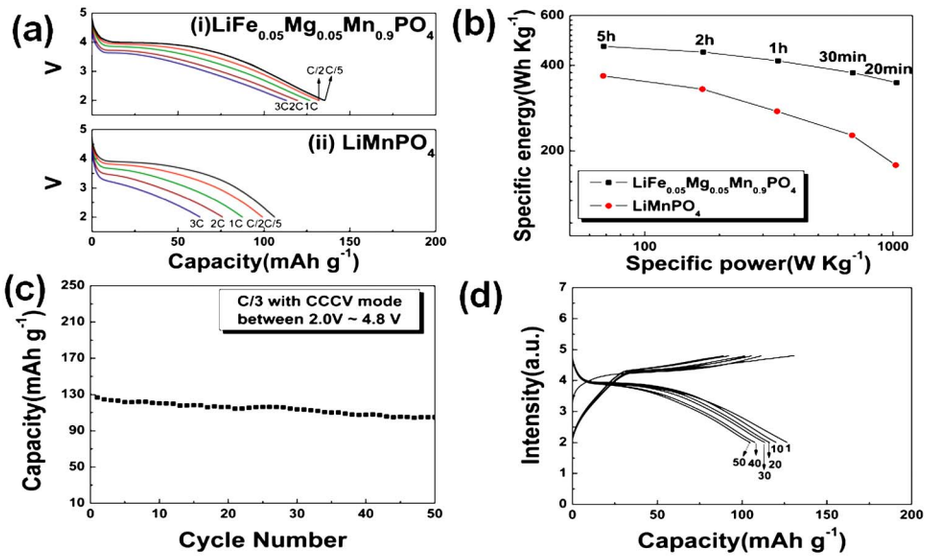


**Figure 4.** (Color online) (a) Rate capability of $LiFe_{0.05}Mg_{0.05}Mn_{0.9}PO_4$ $LiMnPO_4$ from C/5 to 3C; 1C corresponds to about 171 mA $g^{-1}$. (b) The Ragone plot for $LiMnPO_4$ and $LiFe_{0.05}Mg_{0.05}Mn_{0.9}PO_4$. (c) Galvanostatic cyclability data of the 50 cycles for $LiFe_{0.05}Mg_{0.05}Mn_{0.9}PO_4$ between 4.8 and 2 V at a C/3 rate. (d) Corresponding charge/discharge curves of the 50 cycles for $LiFe_{0.05}Mg_{0.05}Mn_{0.9}PO_4$.

$LiFe_{0.05}Mg_{0.05}Mn_{0.9}PO_4$ at elevated current densities are significantly higher than those of $LiMnPO_4$. While the polarization becomes appreciably bigger, therefore rapidly reducing the capacity of the pristine $LiMnPO_4$ at higher current rates, the polarization is comparably smaller for co-doped materials even at 3C. As a result, the discharge capacity of $LiFe_{0.05}Mg_{0.05}Mn_{0.9}PO_4$ at 3C is more than 2 times higher than that of $LiMnPO_4$. It is notable that 10% substitution can dramatically enhance the power capability of $LiMnPO_4$. A Ragone plot for comparison of performance (Fig. 4b) shows that $LiFe_{0.05}Mg_{0.05}Mn_{0.9}PO_4$ retains higher energy density than $LiMnPO_4$ at all discharge rates. This clearly demonstrates that co-doping of Fe–Mg improves the kinetics of Mn based olivine cathode materials.

The cycle property of $LiFe_{0.05}Mg_{0.05}Mn_{0.9}PO_4$ is also investigated to check the stability of the electrode. Figures 4c and 4d show specific capacities and the charge–discharge profile at C/3 for 50 cycles. The results show that high capacity is stably retained at extended cycles. The discharge capacity in the first cycle of ca. 130 mAh $g^{-1}$ only slightly decreases with further cycling. We suspect that the slight capacity fade during cycle is in part due to the instability of the electrolyte when exposed to high potential (4.8 V) for a prolonged time.

To verify the mechanism of the enhanced rate performance of the electrode, we attempted to perform structural analysis on partially delithiated samples using XRD and transmission electron microscopy. The two samples of $Li_{1-x}(FeMg)_{0.05}Mn_{0.9}PO_4$ were prepared at states of (i) and (ii) as denoted in Fig. 5a. At a state (i), the sample is electrochemically charged up to 4.0 V, where $Fe^{2+}$ ions are expected to be fully oxidized. About 30 mAh $g^{-1}$ of Li is extracted from the $LiFe_{0.05}Mg_{0.05}Mn_{0.9}PO_4$ as shown in the profile. Because the charging voltage is lower that the equilibrium redox potential of $Mn^{2+}/Mn^{3+}$ (4.1 V), the capacity is mainly attributed to the $Fe^{2+}/Fe^{3+}$ transition. However, in spite of the delithiation reaction observed at this state, the XRD study could not find any significant change in the pattern (data not shown here). It is possibly due to the small amount of Fe contents and the small size of the second phase nuclei. Instead, particles were further investigated by high resolution transmission electron microscopy (HRTEM). Figure 5b shows an image of partially delithiated $Li_{1-x}(FeMg)_{0.05}Mn_{0.9}PO_4$ at (i), showing clear lattice images. Fast Fourier transform (FFT) of the HRTEM image in Fig. 5c reveals that a new phase has indeed arisen in a single particle of $Li_{1-x}(FeMg)_{0.05}Mn_{0.9}PO_4$ charged to 4.0 V. The formation of a second phase at charging below 4.0 V clearly indi-

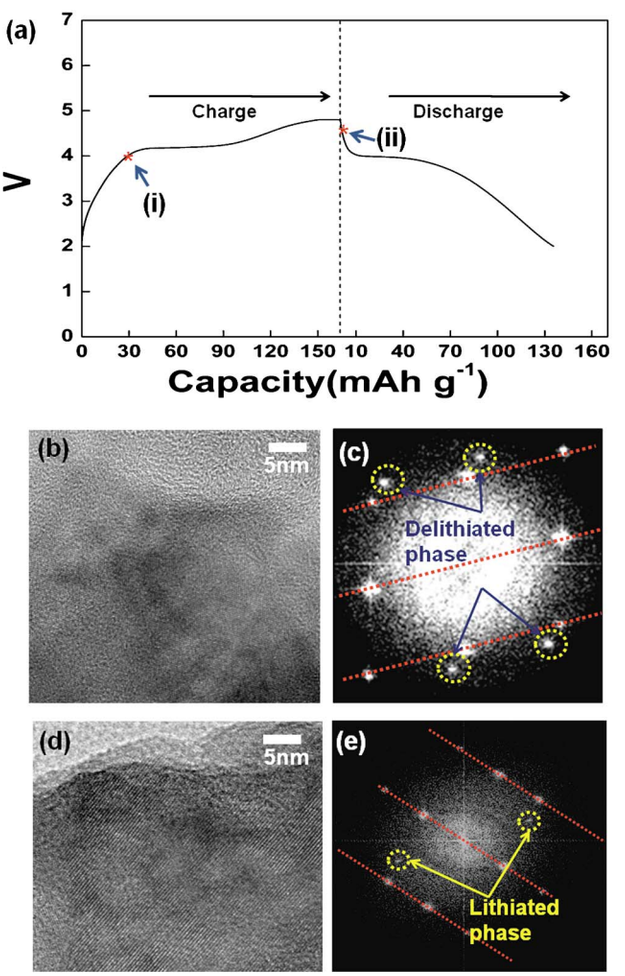


**Figure 5.** (Color online) (a) Charge/discharge profile of $Li_xFe_{0.05}Mg_{0.05}Mn_{0.9}PO_4$ [(i): the charge state of the examined $Li_{1-x}Fe_{0.05}Mg_{0.05}Mn_{0.9}PO_4$; (ii): the discharge state of the examined $Li_xFe_{0.05}Mg_{0.05}Mn_{0.9}PO_4$] (b) Typical HRTEM image of a particle charged up to 0.4 V. (c) Fourier transforms of the Fig. 4b image (yellow circle: delithiated phase), (d) Typical HRTEM image of a particle charging up to 4.8 V, and (e) Fourier transforms of the Fig. 4d image (yellow circle: lithiated phase).

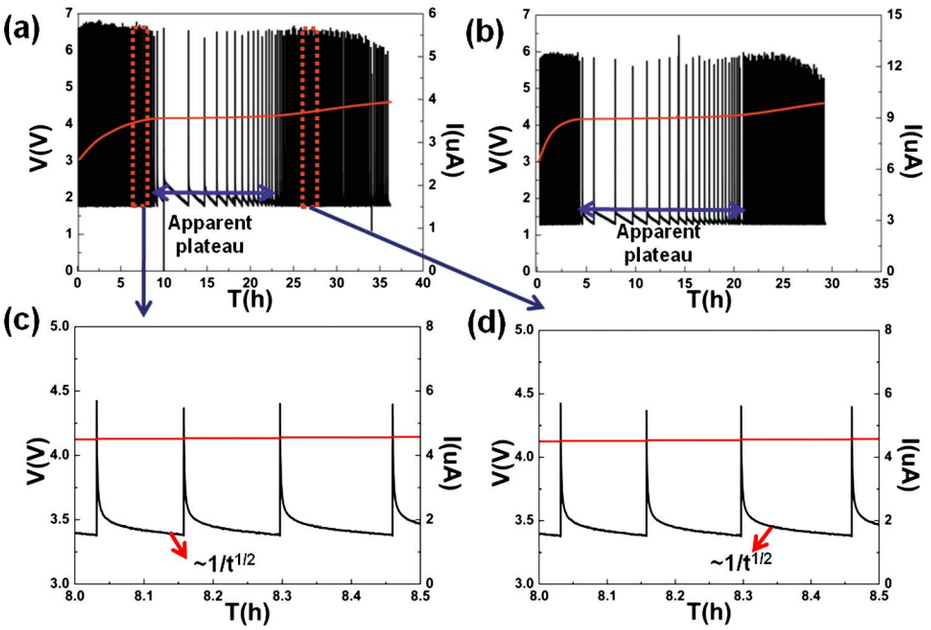


**Figure 6.** (Color online) PITT measurements upon charging of (a) $LiFe_{0.05}Mg_{0.05}Mn_{0.9}PO_4$ and (b) $LiMnPO_4$ from 3 to 4.6 V, and the zoomed PITT profiles of $LiFe_{0.05}Mg_{0.05}Mn_{0.9}PO_4$ (c) between 7 and 10 h and (d) between 21 and 26 h.

cates the existence of multiple nucleation sites provided by Fe redox couple for the $Li^+$ deintercalated phase. This observation is in good agreement with our previous paper.[15]

Additionally, the influence of $Mg^{2+}$ was investigated by analyzing the sample at a (ii) state. At a state (ii), the sample is fully charged up to 4.8 V, as denoted in Fig. 5a. Due to the $Fe^{2+}/Fe^{3+}$ transition at ca. 3.4 V and the $Mn^{2+}/Mn^{3+}$ transition at ca. 4.1 V, all Fe and Mn ions in the sample are expected to be in 3+ in the state (ii). While the similar XRD study on this sample did not find any significant change in the pattern, HRTEM reveals the existence of two phases. Figure 5d shows the continuous lattice images of a sample at (ii). The corresponding FFT of the HRTEM image in Fig. 5e indicates that two phases coexist in a single particle. The lithiated phase is still present even in the fully charged sample at a scale visible to electron beam. We suspect that the presence of Mg in the matrix prevents full delithiation and provides initial sites for the growth of the lithiated phase. It should be noted that investigation of multiple particles yielded the same results.

We further pursued the evidence of facile and multiple nucleations in the co-doped sample by potentiostatic intermittent titration technique experiments. In Fig. 6a and 6b, the PITT voltage steps and corresponding current relaxation curves are compared for $LiFe_{0.05}Mg_{0.05}Mn_{0.9}PO_4$ and $LiMnPO_4$ electrodes. One noticeable observation is that the apparent plateau region significantly shrinks in the $LiFe_{0.05}Mg_{0.05}Mn_{0.9}PO_4$ compared with $LiMnPO_4$. In this plateau region, the current $[I(t)]$ decreases rapidly to a very low value, and then reaches the limit value slowly. This behavior is typically observed in a two-phase reaction.[33,34] However, when we carefully examined the behavior of $I(t)$ at regions before and after the apparent plateaus by zooming in as shown in Fig. 6c and 6d, respectively, a somewhat unexpected phenomenon was observed. The current decay at each step showed a Cottrellian $(1/t^{1/2})$ dependence, which indicates that the process is a solid-solution insertion/extraction reaction.[33,34] This appears to be in contrast to the expected role of Fe and Mg as a nucleation enhancer at a first glance. However, considering that Fe and Mg are extensively distributed in the matrix, and therefore numerous nuclei with very small size (small enough not to be visible by XRD) will be formed and distributed extensively in a matrix, the distinction between solid solution and two phase can be blurred at this scale. The fact that the Cottrellian region significantly increased in the electrochemical profile below and above the equilibrium potential of $Mn^{2+}/Mn^{3+}$ (ca. 4.1 V) reflects that the co-doping alters the nucleation behavior of the second phase in $LiMnPO_4$ framework by inducing "numerous small nucleation" in the matrix or "solid solution."

## Conclusion

The effects of nucleation enhancer on properties of Mn based olivine cathode materials were investigated by co-doping Fe and Mg. The unfavorable $Mn^{2+}$–$V_{Li}$ (or $Mn^{3+}$–$Li^+$) pair neighbors created by local $Fe^{3+}$–$V_{Li}$–$Mn^{2+}$ (or $Mg^{2+}$–$Li^+$–$Mn^{3+}$) regions during $Li^+$ (de)intercalation promote the $Mn^{2+}/Mn^{3+}$ redox transition, where $Fe^{3+}$ (in $Li^+$ deintercalation) and $Mg^{2+}$ (in $Li^+$ intercalation) act as nucleation enhancers. Easier and more frequent nucleation aided by Fe and Mg co-doping enhanced the power capability of Mn based olivine cathode, as evidenced by superior electrochemical performance, a result that is not easily achieved using pristine $LiMnPO_4$ without nucleation enhancers. These results present a direction for future systematic investigation of nucleation enhancers in Mn based olivine cathode materials. We believe that our strategy can be further extended to electrode materials based on a two-phase reaction that have been excluded because of their sluggish kinetics.

## Acknowledgment

This research was supported by the Korea Science and Engineering Foundation (KOSEF) grant funded by the Korea government (MEST) (R11-2008-058-01003-0), the Converging Research Center Program through the National Research Foundation of Korea funded by the Ministry of Education, Science and Technology (NRF-2009-0082069, NRF-2009-0094219). This work was also supported by Energy Resources Technology R&D program (20092020100040) under the Ministry of Knowledge Economy, Republic of Korea.

*KAIST assisted in meeting the publication costs of this article.*

## References

1. P. S. Herle, B. Ellis, N. Coombs, and L. F. Nazar, *Nature Mater.*, **3**, 147 (2004).
2. M. Yonemura, A. Yamada, Y. Takei, N. Sonoyama, and R. Kanno, *J. Electrochem. Soc.*, **151**, A1352 (2004).
3. S. Y. Chung, J. T. Bloking, and Y. M. Chiang, *Nature Mater.*, **1**, 123 (2002).
4. C. Delmas, M. Maccario, L. Croguennec, F. Le Cras, and F. Weill, *Nature Mater.*, **7**, 665 (2008).
5. B. Kang and G. Ceder, *Nature*, **458**, 190 (2009).
6. A. K. Padhi, K. S. Nanjundaswamy, C. Masquelier, S. Okada, and J. B. Goodenough, *J. Electrochem. Soc.*, **144**, 1609 (1997).
7. A. K. Padhi, K. S. Nanjundaswamy, and J. B. Goodenough, *J. Electrochem. Soc.*, **144**, 1188 (1997).

8. S. Nishimura, G. Kobayashi, K. Ohoyama, R. Kanno, M. Yashima, and A. Yamada, *Nature Mater.*, **7**, 707 (2008).
9. C. Delacourt, P. Poizot, J.-M. Tarascon, and C. Masquelier, *Nature Mater.*, **4**, 254 (2005).
10. A. Yamada, M. Hosoya, S.-C. Chung, Y. Kudo, K. Hinokuma, K.-Y. Liu, and Y. Nishi, *J. Power Sources*, **119–121**, 232 (2003).
11. F. Zhou, M. Cococcioni, K. Kang, and G. Ceder, *Electrochem. Commun.*, **6**, 1144 (2004).
12. C. Delacourt, L. Laffont, R. Bouchet, C. Wurm, J. B. Leriche, M. Morcrette, J. M. Tarascon, and C. Masquelier, *J. Electrochem. Soc.*, **152**, A913 (2005).
13. G. H. Li, H. Azuma, and M. Tohda, *Electrochem. Solid-State Lett.*, **5**, A135 (2002).
14. D. W. Choi, D. H. Wang, I. T. Bae, J. Xiao, Z. M. Nie, W. Wang, V. V. Viswanathan, Y. J. Lee, J. G. Zhang, G. L. Graff, et al., *Nano Lett.*, **10**, 2799 (2010).
15. J. Kim, D. H. Seo, S. W. Kim, Y. U. Park, and K. Kang, *Chem. Commun.*, **46**, 1305 (2010).
16. T. Shiratsuchi, S. Okada, T. Doi, and J. Yamaki, *Electrochim. Acta*, **54**, 3145 (2009).
17. H. S. Fang, L. P. Li, Y. Yang, G. F. Yan, and G. S. Li, *Chem. Commun.*, **2008**, 1118.
18. S. K. Martha, B. Markovsky, J. Grinblat, Y. Gofer, O. Haik, E. Zinigrad, D. Aurbach, T. Drezen, D. Wang, G. Deghenghi, et al., *J. Electrochem. Soc.*, **156**, A541 (2009).
19. D. Y. Wang, H. Buqa, M. Crouzet, G. Deghenghi, T. Drezen, I. Exnar, N. H. Kwon, J. H. Miners, L. Poletto, and M. Graetzel, *J. Power Sources*, **189**, 624 (2009).
20. Z. Bakenov and I. Taniguchi, *J. Power Sources*, **195**, 7445 (2010).
21. B. Kang and G. Ceder, *J. Electrochem. Soc.*, **157**, A808 (2010).
22. K. Saravanan, J. J. Vittal, M. V. Reddy, B. V. R. Chowdari, and P. Balaya, *J. Solid State Electrochem.*, **14**, 1755 (2010).
23. D. Y. Wang, C. Y. Ouyang, T. Drezen, I. Exnar, A. Kay, N. H. Kwon, P. Gouerec, J. H. Miners, M. K. Wang, and M. Gratzel, *J. Electrochem. Soc.*, **157**, A225 (2010).
24. J. Xiao, W. Xu, D. W. Choi, and J. G. Zhang, *J. Electrochem. Soc.*, **157**, A142 (2010).
25. J. J. Chen, M. J. Vacchio, S. J. Wang, N. Chernova, P. Y. Zavalij, and M. S. Whittingham, *Solid State Ionics*, **178**, 1676 (2008).
26. H. Gwon, D. H. Seo, S. W. Kim, J. Kim, and K. Kang, *Adv. Funct. Mater.*, **19**, 3285 (2009).
27. D. H. Seo, H. Gwon, S. W. Kim, J. Kim, and K. Kang, *Chem. Mater.*, **22**, 518 (2010).
28. Y.-U. Park, J. Kim, H. Gwon, D. H. Seo, S. W. Kim, and K. Kang, *Chem. Mater.*, **22**, 2573 (2010).
29. S.-W. Kim, J. Kim, H. Gwon, and K. Kang, *J. Electrochem. Soc.*, **156**, A635 (2009).
30. C. Delacourt, P. Poizot, M. Morcrette, J. M. Tarascon, and C. Masquelier, *Chem. Mater.*, **16**, 93 (2004).
31. F. Zhou, T. Maxisch, and G. Ceder, *Phys. Rev. Lett.*, **97**, 155704 (2006).
32. R. Malik, F. Zhou, and G. Ceder, *Phys. Rev. B*, **79**, 214201 (2009).
33. N. Meethong, Y. H. Kao, W. C. Carter, and Y. M. Chiang, *Chem. Mater.*, **22**, 1088 (2010).
34. M. Jiang, B. Key, Y. S. Meng, and C. P. Grey, *Chem. Mater.*, **21**, 2733 (2009).